ACS OMEGA

http://pubs.acs.org/journal/acsodf

Article

Comparative Analyses between Raw and Preoxidized Pulverized Coals: Combustion Behaviors and Thermokinetic and Microcharacteristics

Li Zou, Yungang Wang,* Yanyuan Bai, Yang Liu, and Qinxin Zhao

Cite This: *ACS Omega* 2022, 7, 1121−1131

Read Online

ACCESS | Metrics & More | Article Recommendations

ABSTRACT: Investigating the difference in the combustion performance and microcharacteristics of oxidized and raw pulverized coal (PC) can contribute to effectively prevent and control the spontaneous combustion of deposited coal dust in high-temperature environment and further help guarantee the safe operation of coal-fired boiler. In this study, the combustion performance and thermokinetic and microcharacteristics of three raw coal samples and their preoxidized forms were explored by a thermogravimetric analyzer (TGA) and Fourier transform infrared spectroscopy (FTIR). According to the characteristic temperatures and variations of the mass loss rate during heating, the entire combustion process of PC was divided into four periods. For each type of coal, the preoxidized PC had relatively lower characteristic temperatures than the corresponding raw PC. The preoxidized samples had larger values of ignition index (C_{ig}) and comprehensive combustibility index (S), but lower values of burnout index (C_b) than raw samples. The values of apparent activation energy (E) for the preoxidized PC were below that of the corresponding raw PC at the same conversion rate (α), which suggested the preoxidized PC required relatively less energy to react and was more prone to spontaneous combustion. In addition, although parts of −OH, C═O, and aliphatic hydrocarbon groups were consumed after the preoxidation treatment, the increase in C−O and −COO− bonds compensated for the adverse effect of the reduction of the aforementioned groups on coal combustion.

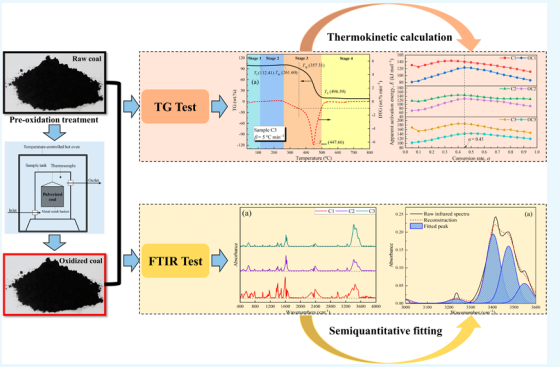

1. INTRODUCTION

As one of the fundamental fossil fuels, coal resource accounts for more than 50% of the primary energy consumption in China.[1,2] To reach the purposes of cleanliness and high efficiency, coal is extensively utilized in thermal power, metallurgy and chemical industries, etc. in the form of a powder.[3] The pulverized coal (PC) is more prone to react with oxygen and generate heat contrasting with lump coal, which is because the PC has a lesser particle size and larger specific surface area.[4,5] Thus, PC also has relatively greater self-ignition hazard than lump coal. In general, coal needs to be milled into PC and dried before entering the industrial boiler for achieving maximum combustion performance.[6,7] However, such precrushing and predrying treatment can remarkably change the physicochemical property of coal, further enhancing its thermal reactivity.[8]

The undesired PC accumulation frequently occurs in the milling system of the coal-fired boiler, such as the outlet of the coal mill and the coarse powder separator. Generally, to boost the thermal efficiency of the boiler and prevent sticking of PC in the air powder pipeline, the outlet temperature of the coal mill is often increased to 80 °C or even about 100 °C.[9] This coal dust will be further oxidized after contact with hot air for a long time. The research of Deng et al. suggested that the secondary oxidation PC had a larger reactivity than raw PC.[10] Thus, the possibility of self-ignition and even explosion of piled PC increases dramatically, which poses a severe threat for equipment-safe operation. Furthermore, the coal dust piled in the coal warehouse for a long time can also be oxidized, and the self-ignition hazard increases if these oxidized PCs are directly utilized. Hence, it is necessary to understand the self-ignition characteristics for preoxidized pulverized coal.

There are various flammable and explosive gases (CO_2, CH_4, C_2H_4, C_2H_6, etc.) generated during PC spontaneous combustion accompanied by heat release, which can cause the wastage of resources and a threat to the environment.[11,12] They even trigger a PC blast accident and further result in equipment damage and casualties. Therefore, understanding the combus-

Received: October 12, 2021
Accepted: November 26, 2021
Published: December 20, 2021

https://doi.org/10.1021/acsomega.1c05694
ACS Omega 2022, 7, 1121−1131

tion behavior and self-ignition hazard of PC, especially oxidized PC, is perfectly imperative for guaranteeing security production. Zhang et al.[13] contrasted the self-ignition limiting parameters of primary and secondary oxidation for three types of coals and found that the secondary oxidation has a lower minimum floating coal thickness and limiting oxygen concentration, as well as a greater maximum air leakage intensity than primary oxidation, indicating that the self-ignition risk increased after secondary oxidation. Deng et al.[14] investigated the thermal properties of four types of coal after reoxidation and found that the hazard of spontaneous combustion of reoxidation was greater than that of primary oxidation. Tang et al.[15] studied the characteristics of secondary oxidation for two types of lignite coals and suggested that the secondary oxidation caused microstructural variations in coal and increased the self-ignition hazard, whereas the preoxidation treatment at an excessively high temperature (>175 °C) might overconsume the organic components, declining the liability of spontaneous combustion. All of these investigations focused on the reoxidation characteristics of coal, whereas the combustion performance, thermokinetic, and main functional group variation related to PC self-ignition of raw and preoxidized coal have not been completely explained. Therefore, further research is still essential.

In this study, combustion behaviors and microstructures of three types of coal were investigated using a thermogravimetric analyzer (TGA) and Fourier transform infrared spectroscopy (FTIR), respectively. Several characteristic parameters were utilized to contrast the combustion performances of raw and preoxidized PC. In addition, the distributed activation energy model (DAEM) method was adopted to study the thermokinetic behaviors of raw and preoxidized samples during pyrolysis and combustion. The abovementioned researches can further facilitate the understanding for the difference in self-ignition evolution between oxidized and raw PC and also provide limited theoretical guidance for the safe operation of coal-fired boiler.

2. EXPERIMENTS AND METHODS

2.1. Sample Preparation. Three coal samples with different ranks were collected from Changzhi coal mine in Shanxi province (C1), Yanzhou coal mine in Shandong province (C2), and Zhangjiamao coal mine in Shaanxi province (C3). These samples were crushed by a coal mill in N_2 ambience, and sieved into dust with a diameter of less than 200-mesh (<74 μm) for being consistent with the on-site situation. Furthermore, these three samples were oxidized by a temperature-controlled hot oven (Figure 1) at 100 °C for 5 h under air atmosphere and utilized as preoxidized samples. These preoxidized samples were named OC1, OC2, and OC3, respectively (i.e., the corresponding preoxidized sample of C1 is OC1, and so on). Both raw and preoxidized PC were kept sealed before experiments.

2.2. Proximate and Ultimate Tests. The moisture, ash, volatile, and fixed carbon contents of raw PC were defined by a 5E-MAG6700 proximate analyzer (Kaiyuan, China) according to GB/T212-2008. The C, H, N, S, and O contents of samples were determined using a vario EL cube element analyzer (Elementar, Germany) according to GB/T214-2007. In addition, the heating value was determined by an oxygen bomb calorimeter (IKA-C200, Germany) following the Chinese National Standard GB/T 213-2008. Notably, FC_{ad} was determined using the subtraction method and compared with the contents of A_{ad}, M_{ad}, and V_{ad}. The O content was defined by the subtraction method and compared with the contents of C, H, N, S, M_{ad}, and A_{ad}.

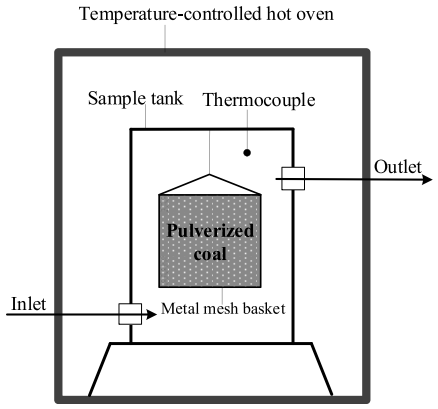

Figure 1. Schematic diagram of hot oven apparatus.

2.3. Thermogravimetric Test. In the thermal analysis tests, a Pyris 1 TGA thermal analyzer (PerkinElmer) with a sensitivity of 10^{-7} g was utilized to measure the characteristic parameters (e.g., mass loss, mass loss rate, and characteristic temperature) during the oxidation process of PC. According to the requirements of experimental apparatus, the initial mass of PC sample transferred into the reaction bed was roughly 6 mg. The samples were heated from 30 to 800 °C at various heating rates (5, 10, 15, and 20 °C min^{-1}). These samples were tested in air atmosphere and the flow rate was 40 mL min^{-1}.

2.4. Fourier Transform Infrared Spectroscopy (FTIR) Test. In this work, a Bruker VERTEX 70 FTIR spectrometer (Bruker, Germany) was adopted to measure the forms and intensities of active functional groups of both raw and preoxidized PC. The KBr tableting method was utilized, and first the PC sample and dry KBr powder were ground with a mass ratio of 1:180. After the grinding process was completed, the mixture-doped KBr powder and PC were transferred in a hollow cylinder mold, and then this mold was placed on a tablet press with 20 MPa for 10 min immediately. Lastly, these tablet samples were tested by the FTIR spectrometer under air atmosphere. In addition, the wavenumber range in this experiment was 4000−400 cm^{-1}, with a resolution of 4.0 cm^{-1}, and the total number of scans was 32.

2.5. Determination of Combustion Performance Parameters. In this study, the ignition index (C_{ig}, % min^{-3}) and burnout index (C_b, % min^{-4}) were applied to evaluate the ignition and burnout performance of PC, respectively. Both the parameters are described in eqs 1 and 2 as follows, respectively[16,17]

$$C_{ig} = \frac{DTG_{max}}{t_{ig} t_{max}} \quad (1)$$

$$C_b = \frac{DTG_{max}}{\Delta t_{1/2} t_{max} t_b} \quad (2)$$

where DTG_{max} is the maximum mass loss rate (% min^{-1}); t_{ig} and t_{max} are the corresponding times of T_{ig} and DTG_{max}, respectively (min); t_b is the burnout time (min); and $\Delta t_{1/2}$ is the time zone of $DTG/DTG_{max} = 1/2$ (min).

In addition, the comprehensive combustibility index (S, $\%^2$ $°C^{-3}$ min^{-2}) can represent the combustion performance of PC.[18] Generally, a higher S value suggests more satisfactory combustion performance. S value can be calculated by eq 3

https://doi.org/10.1021/acsomega.1c05694
ACS Omega 2022, 7, 1121−1131

Table 1. Proximate and Ultimate Analyses of raw PC

	proximate analysis (wt %)					ultimate analysis (wt %)					
sample	M_{ad}	A_{ad}	V_{ad}	FC_{ad}	FC_{ad}/V_{ad}	C	H	O	N	S	HHV (MJ kg^{-1})
C1	1.92	11.52	27.22	59.34	2.14	79.31	3.22	2.58	0.83	0.62	30.41
C2	2.06	8.75	38.28	50.91	1.33	77.89	4.93	4.03	1.82	0.52	26.38
C3	2.86	9.78	41.56	45.80	1.10	74.11	4.61	6.70	1.78	0.16	25.74

Note: ad, air dry basis; M, moisture; A, ash; V, volatile matter; FC, fixed carbon; HHV, higher heating value.

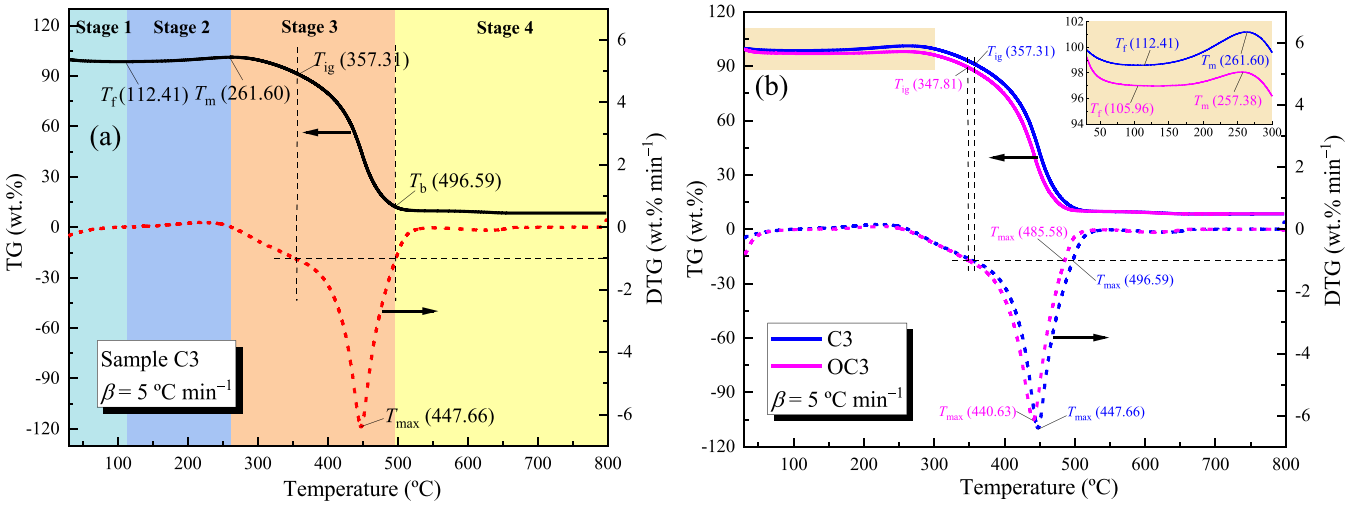

Figure 2. TG/DTG curves during oxidation combustion at a heating rate of 5 °C min^{-1}: (a) C3 and (b) C3 vs OC3.

$$S = \frac{DTG_{max}DTG_{ave}}{T_{ig}^2 T_b} \quad (3)$$

where DTG_{ave} is the average mass loss rate (% min^{-1}) and T_{ig} and T_b are the ignition temperature and burnout temperature, respectively (°C).

2.6. Thermokinetic Analysis Method. To analyze intricate reactions such as pyrolysis of fossil fuels, sludge, biomass and their mixtures, etc., the DAEM method has been widely adopted based on the assumption that the entire reaction process is constituted of a series of irreversible independent and parallel first-order decomposition reactions.[19,20] The model is described as follows when it is utilized to represent the change in the total evolved volatiles (V) against time (t) during nonisothermal pyrolysis of solid fuels

$$1 - \frac{V}{V^*} = \int_0^\infty \exp\left[-A\int_0^t \exp\left(-\frac{E}{RT}\right)dt\right] f(E)dE \quad (4)$$

where V and V^* represent the total volatiles evolved by time t and the effective volatiles of the sample, respectively; A is the preexponential factor (s^{-1}); E is the apparent activation energy (kJ mol^{-1}); t is the reaction time (min); and $f(E)$ is the normalized distribution curve of the apparent activation energy, which can be obtained through graphically differentiating V/V^* by E.

Considering that the PC combustion has a similar mass loss curve to PC pyrolysis on the basis of TG, the DAEM method is further utilized to analyze the entire combustion process of PC in this work. Equation 4 can be rewritten as follows, assuming the combustion process of PC is constituted of a variety of first-order oxidation reactions[21]

$$1 - \alpha = \int_0^\infty \exp\left[-A\int_0^t \exp\left(-\frac{E}{RT}\right)dt\right] f(E)dE \quad (5)$$

where α is the conversion rate of PC by time t ($0 < \alpha < 1$). Then, an isoconversional method is applied to calculate the thermokinetic parameters during PC combustion referencing to Miura–Maki, based on different groups of TG data at multiple heating rates.[22] This method can directly obtain the thermokinetic parameters simultaneously without assuming specific A and $f(E)$, and is described as follows

$$\ln\left(\frac{\beta_i}{T_{\alpha,i}^2}\right) = -\frac{E_\alpha}{RT_\alpha} + \ln\left(\frac{A_\alpha R}{E_\alpha}\right) + 0.6075 \quad (6)$$

where β_i is the heating rate (°C min^{-1}); $T_{\alpha,i}$ is the PC temperature at conversion rate "α" and heating rate "i" (K); and R is the gas constant (whose value is 8.314 J mol^{-1} K^{-1}).

3. RESULTS AND DISCUSSION

3.1. Proximate and Ultimate Analyses. The results of proximate and ultimate analyses of raw samples are listed in Table 1. It was clear that the moisture contents of the PC were all relatively low, and the detailed values of samples C1, C2, and C3 were 1.92, 2.06, and 2.86 wt %, respectively. Generally, fuel ratio (i.e., FC_{ad}/V_{ad}) is an effective index to define the maturity of the coal sample, and a higher value represents a high coal rank. Therefore, the rank of these three PCs is as follows: C1 > C2 > C3. The ash contents of samples C1, C2, and C3 were 11.52, 8.75, and 9.78 wt %, respectively. Both volatile and O contents can remarkably affect the combustion characteristics of PC, and their values all decreased gradually with the increase of coal rank. Notably, prominent differences were determined between the fixed carbon contents of PC samples, which were 59.34 (C1), 50.91 (C2), and 45.80 (C3) wt %. In addition, the higher

https://doi.org/10.1021/acsomega.1c05694
ACS Omega 2022, 7, 1121−1131

Table 2. Characteristic Parameters of PC at a Heating Rate of 5 °C min^{-1}

	sample					
characteristic parameters	C1	OC1	C2	OC2	C3	OC3
T_f (°C)	177.12	168.31	130.65	124.35	112.41	105.96
T_m (°C)	337.52	328.15	273.03	261.24	261.60	257.38
T_{ig} (°C)	423.06	410.50	389.24	376.21	357.31	347.81
T_{max} (°C)	490.71	478.39	450.11	439.51	447.66	440.63
T_b (°C)	543.14	538.15	510.44	502.36	496.59	485.58
stage 1 mass loss (wt %)	0.54	0.34	1.35	1.05	1.39	3.01
stage 2 mass gain (wt %)	4.38	2.51	2.69	1.26	2.58	1.08
stage 3 mass loss (wt %)	88.22	87.24	90.48	88.34	86.37	85.48
stage 4 mass loss (wt %)	4.93	3.95	2.82	2.06	6.35	3.41
total mass loss (wt %)	89.31	89.02	91.96	90.19	91.53	90.82

heating values of coal samples C1, C2, and C3 were 30.41, 26.38, and 25.74 MJ kg^{-1}, respectively, i.e., increasing gradually with the increase of coal rank.

3.2. TG/DTG Analysis. Figure 2a describes TG/DTG curves of sample C3 during oxidation combustion at a heating rate of 5 °C min^{-1}, and these curves are utilized to identify the characteristic temperatures during the oxidation combustion of PC. Five characteristic temperature points (i.e., T_f, T_m, T_{ig}, T_{max}, and T_b) were observed in the TG and DTG curves, which were consistent with the results obtained by Deng et al.[23] T_f, T_m, and T_{max} represented the corresponding temperatures of the maximum water evaporation and gas desorption, maximum oxidization mass gain, and maximum mass loss rate, respectively. Meanwhile, T_{ig} and T_b indicated the temperatures of ignition and burnout, and their detailed values were defined as the temperature where the mass loss rate is 1 wt % min^{-1} at the initial phase of combustion and at the final phase of the combustion, respectively.[24] According to these characteristic temperatures and variation of TG/DTG curves, the entire combustion process of the PC sample was separated into four periods: water evaporation and gas desorption (stage 1), oxygen absorption mass gain (stage 2), pyrolysis and combustion (stage 3), and burnout (stage 4).

Figure 2b contrasts the differences of TG/DTG plots between C3 and its preoxidized sample OC3 during oxidation combustion with a heating rate of 5 °C min^{-1}. Both TG and DTG curves of these two PCs had a fully similar variation when the temperature was approximately below 200 °C, which ascribed mainly the relatively low coal temperature and oxygen reaction intensity. Both T_f and T_m values of sample OC3 (105.96 and 257.38 °C) were all less than those of C3 (112.41 and 261.60 °C). However, the differences were relatively lower, which represented the preoxidation treatment had a mild effect on the initial stage of PC combustion. Subsequently, the oxidation reaction rate increased gradually as the temperature increased steadily, which resulted in a tiny decrease in mass from TG curves. Meanwhile, devolatilization and PC pyrolysis were also pivotal routes that caused the decrease in mass. The mass of these two samples decreased steeply when the coal temperature surpassed T_{ig}, which indicated that the PC samples entered into the rapid combustion stage. At this period, the mass loss rate attained the maximum through a tiny time. The T_{ig} values of samples C3 and OC3 were 357.31 and 347.81 °C, respectively, differing by about 9.50 °C. In addition, the T_{max} value of OC3 (440.63 °C) was less than that of C3 (447.66 °C). Generally, the moisture content can influence the heat transfer efficiency of PC, and the evaporation of moisture can also consume some heat. Therefore, sample OC3 reached the T_{ig} and T_{max} earlier than sample C3. In addition, a portion of steady groups existing in the PC can also be activated as activation molecules that reacted easily with oxygen upon the preoxidation treatment, which suggested that sample OC3 can be ignited more readily than C3.

Table 2 presents the detailed data regarding characteristic temperatures of raw and preoxidized PC based on TG/DTG curves at a heating rate of 5 °C min^{-1}. Sample C1 displayed the largest characteristic temperatures (including T_f, T_m, T_{ig}, T_{max}, and T_b) in these three raw samples, followed by sample C2, and the values of sample C3 were the minimum. That is, these characteristic temperatures increased with the increase in coal rank. A higher thermal maturity of coal suggested the stronger aromatized structures and more stable functional groups.[25] Thus, the whole TG curve of sample C1 moved to a high-temperature area. In addition, the volatile matter in coal is the easiest substance to ignite and the combustion of the volatile matter is the first step during the whole oxidation combustion. Therefore, the characteristic temperatures were fundamentally related to the volatile matter of coal, i.e., with the decrease in volatile matter, the characteristic temperatures were larger. Table 1 indicates that the volatile matter of sample C1 is the least and consequently marked by highest characteristic temperatures. The T_m values of these six samples ranged from 257.38 to 337.52 °C, and the T_m values of samples OC1−OC3 (328.15, 261.24, and 257.38 °C) were all mildly lower than those of their corresponding raw samples (337.52, 273.03, and 261.60 °C). After the preoxidation treatment, a portion of the adsorption sites in coal was occupied by oxygen molecules; thus, the preoxidation samples attained the peak values of oxidization mass gain earlier than their raw samples. For the three coal samples, the differences of T_{ig} values between raw and preoxidized samples were 12.56 °C (C1 vs OC1), 13.03 °C (C2 vs OC2), and 9.50 °C (C3 vs OC3), which represented that the preoxidation treatment had a high influence on T_{ig}. T_{ig} is a remarkable index mirroring the difficulty degree of PC combustion, and its low value suggests that PC is easier to be ignited. Therefore, the preoxidized samples were more prone to be ignited than the raw samples. The T_{max} values of samples C1, OC1, C2, OC2, C3, and OC3 were 490.71, 478.39, 450.11, 439.51, 447.66, and 440.63 °C, respectively; meanwhile, the T_b values were 543.14, 538.15, 510.44, 502.36, 496.59, and 485.58 °C, respectively. It is transparent that the T_{max} and T_b values of preoxidized coal were all lower than those of raw coal.

Table 2 also displays the mass variation at each stage in the process of PC oxidation combustion. The values of mass loss in stages 1, 2, 3, and 4 ranged from 0.34 to 3.01, 1.08 to 4.38, 85.48 to 90.48, and 2.06 to 6.35 wt %, respectively. For both samples OC1 and OC2, their mass loss values at stage 1 were mildly

https://doi.org/10.1021/acsomega.1c05694
ACS Omega 2022, 7, 1121−1131

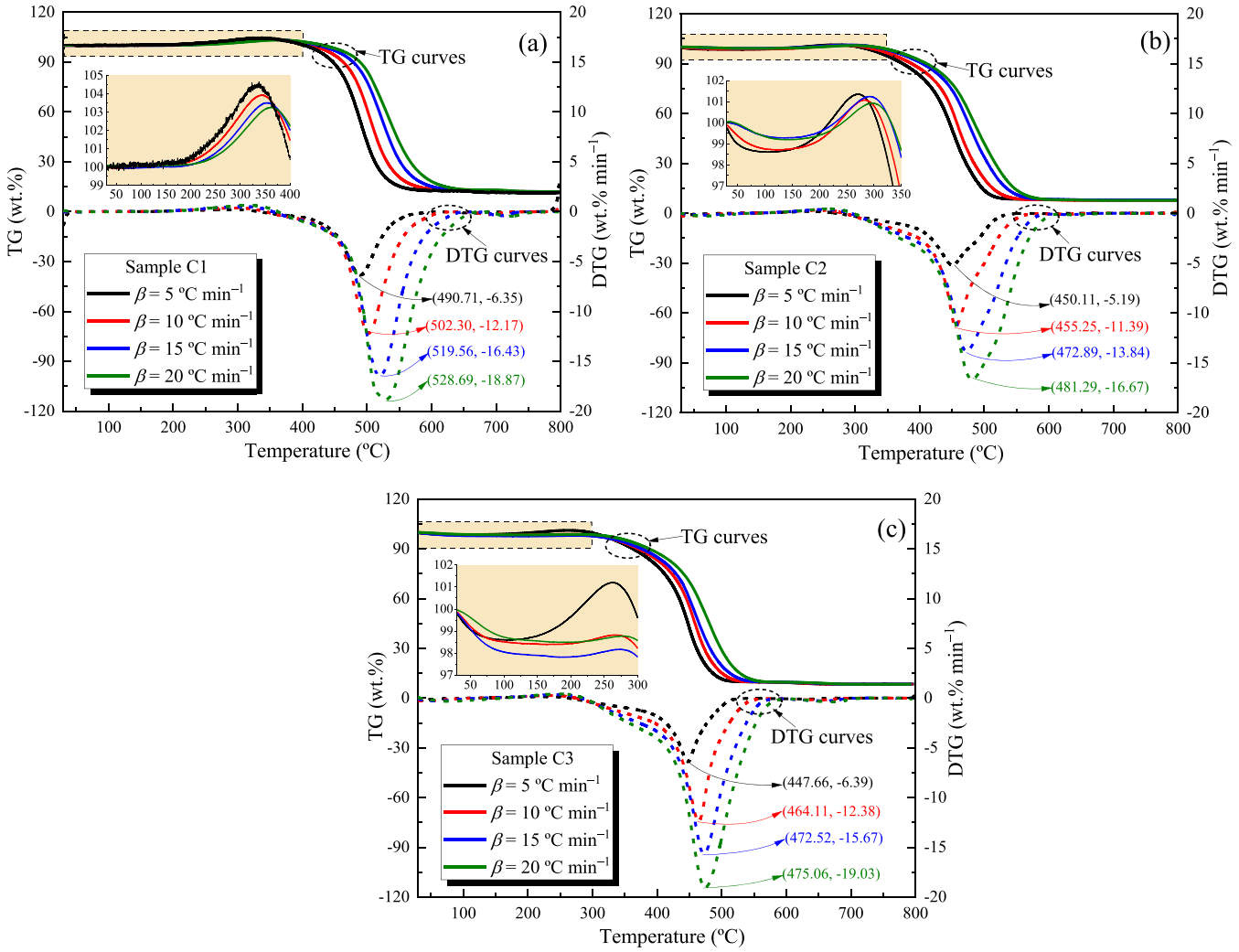

Figure 3. TG/DTG curves of PC during oxidation combustion at various heating rates, (a) C1, (b) C2, and (c) C3.

Table 3. Combustion Performance Parameters of PC at 5 °C min^{-1}

sample	DTG_{max} (wt % min^{-1})	DTG_{ave} (wt % min^{-1})	$C_{ig} \times 10^4$ (wt % min^{-3})	$C_b \times 10^5$ (wt % min^{-4})	$S \times 10^8$ (wt %^{2} °C^{-3} min^{-2})
C1	6.35	0.58	7.65	5.23	3.79
OC1	6.05	0.56	7.70	4.68	3.84
C2	5.19	0.60	7.41	3.91	4.03
OC2	4.97	0.59	7.51	3.69	4.12
C3	6.39	0.59	9.89	7.39	5.95
OC3	6.13	0.58	10.02	6.80	6.05

below those of the corresponding raw samples due to the decrease in moisture content. However, sample OC3 had a larger mass loss at stage 1 than that of sample C3, which might be related to the instability of the TG test at a lower temperature. Moreover, due to the decrease in oxygen adsorption sites of coal after the preoxidation treatment, the mass gain at stage 2 of the preoxidized samples was also lower than that of their raw samples. For all PC samples, maximum mass losses were observed at stage 3, illustrating that vigorous ignition occurred at this phase. Thus, a thermokinetic analysis method was adopted in this work to evaluate the thermokinetic behavior of stage 3, as shown in Section 3.4. Notably, a tiny mass loss was observed at stage 4 because of the high-temperature pyrolysis of coke and ash.[26] The total mass losses of samples C1, OC1, C2, OC2, C3, and OC3 were 89.31, 89.02, 91.96, 90.19, 91.53, and 90.82 wt % respectively, which were mainly consistent with the fixed carbon and volatile contents. Nevertheless, the PC weight utilized in the TG test was relatively low (about 6 mg) and cannot absolutely denote the actual state. Therefore, conducting a larger-scale simulation experiment or a field industrial test was essential for acquiring the precise results regarding the combustion process of PC.

To explore the influence of the heating rate on the combustion process of PC, TG/DTG curves of three raw PC samples at various heating rates were analyzed, as described in Figure 3. TG/DTG plots of the three samples moved to a high-temperature area gradually as the heating rate increased. DTG curves of PC at various heating rates displayed highly similar tendencies when the temperature was below T_{ig}; however, remarkable differences between these DTG curves were

https://doi.org/10.1021/acsomega.1c05694
ACS Omega 2022, 7, 1121−1131

observed after combustion. When the heating rate increased from 5 to 20 °C min^{-1}, the increase of maximum mass loss rate and corresponding temperature of samples C1, C2, and C3 were 12.52 wt % and 37.98 °C, 11.48 wt % and 31.18 °C, and 12.64 wt % and 27.40 °C, respectively. On the one hand, the increase in heating rate can shorten the contact time of PC and oxygen and cause incomplete reaction between the active structure in coal and oxygen, and eventually resulted in the delay of the combustion process of PC. On the other hand, the number and types of complexes generated on the surface of PC at different heating rates were also different. At the condition of higher heating rate, the functional groups that did not oxidize in time at the previous phase participated in PC combustion, causing a heterogeneous ignition, which delayed the combustion process of PC.[27]

3.3. Analysis of Combustion Performance Parameters. Three parameters (C_{ig}, C_b, and S) were calculated according to eqs 1−3 for evaluating the combustion performance of PC, and the detailed values are presented in Table 3. The DTG_{max} values of samples OC1, OC2, and OC3 (i.e., 6.05, 4.97, and 6.13 wt % min^{-1}, respectively) were all lower than those of their raw samples (6.35, 5.19, and 6.39 wt % min^{-1} respectively), which suggested that the preoxidized samples had relatively lower volatile release and combustion mass loss at T_{max} than raw samples because a part of combustibles were consumed during the preoxidation treatment.[28] Meanwhile, DTG_{ave} values of preoxidized samples were also observed to be lower than those of raw PC. The C_{ig} and S values of preoxidized PC were all greater than those of their corresponding raw PC. However, the values of C_b for preoxidized PC were observed to be lower than those of the corresponding raw samples. Generally, a high C_{ig} represents that the PC is readily ignited and a high C_b can result in a lengthened combustion process.[29] Thus, the preoxidation samples were more prone to self-ignition but had a shorter combustion stage. In addition, the higher S of OC1, OC2, and OC3 also suggested that the preoxidized samples can be ignited and burnt-out at lower temperatures compared with raw samples.

3.4. Thermokinetic Analysis. The thermokinetic parameters of the pyrolysis and combustion region (stage 3) from T_m to T_b were investigated using the DAEM method in this work. The plots of conversion rate α vs PC temperature were described from TG data, and the temperature at the selected α could be gained for each heating rate. Moreover, the linear correlations of $\ln(\beta/T^2)$ vs $1/T$ were established according to eq 6. The apparent activation energy (E) and preexponential factor (A) were reckoned according to the linearization process at four different heating rates, and the results of α vs E are depicted in Figure 4. The E values of these six samples increased gradually and then decreased with the increase in α, the maximum was observed at $\alpha = 0.45$ (i.e., nearby T_{max}), which was different from PC pyrolysis. At the initial stage ($\alpha < 0.45$), PC pyrolysis and combustion mainly depended on the external heat; thus, the required heat kept increasing with the increase in reaction intensity of combustion, i.e., E increased as α increased. Nevertheless, the PC burned violently and released a lot of heat when the α value was greater than 0.45, which resulted in the decrease of required external heat, i.e., E decreased as α increased. Interestingly, E values of the three preoxidized PC were all lower than their corresponding raw samples at the same α, which suggested that the preoxidized sample can be ignited by absorbing lower heat than the raw sample. In other words, the preoxidized PC had a relatively higher self-ignition hazard than

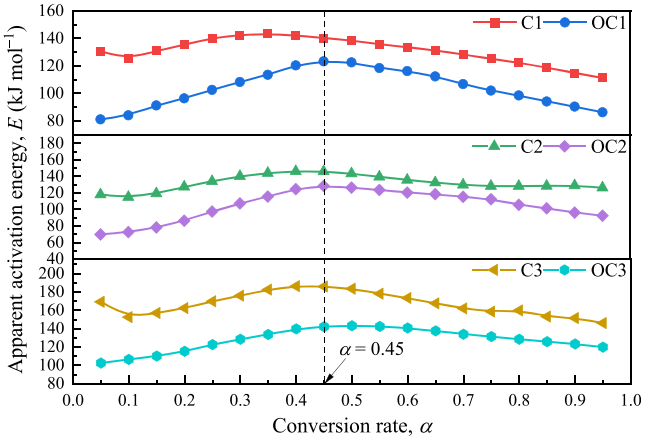

Figure 4. Relationship between α and E determined from the Miura−Maki method for the pyrolysis and combustion process of raw and preoxidized PC.

raw PC. Notably, the thermokinetic analysis should be utilized only as a reference because of the low sample mass (about 6 mg) and the different temperature areas at stage 3 between raw and preoxidized samples in the TG test; further research was essential for obtaining more details regarding the combustion behavior of raw and preoxidized PC, such as the self-ignition test of accumulated PC at a thermostatic condition, etc.

Graphically differentiating α from E, we can gain E distribution $f(E)$ as described in Figure 5. For each PC sample, the pyrolysis and combustion process described an approximate Gaussian distribution with the increase of α. The peak value of $f(E)$ was more centralized around $\alpha = 0.45$ (i.e., nearby T_{max}), indicating that there was highest reaction intensity near T_{max}. Further observation demonstrated that the corresponding E of the maximum $f(E)$ of OC1, OC2, and OC3 (122.60, 126.50, and 142.36 kJ mol^{-1}) were all lower than those of corresponding raw samples (142.46, 145.96, and 185.91 kJ mol^{-1}), respectively, which further proved the preoxidized PC was more prone to be ignited than raw PC. As for samples C2, OC2, C3, and OC3, both distinct abundance distributions of E might represent two partial reactions during pyrolysis and combustion. In partial reaction 1, the burning of numerous volatile matter and fixed carbon released a large amount of heat and various gaseous products, meanwhile accompanied by the burning of char at a higher temperature, whereas partial reaction 2 was mainly related to the combustion of small amounts of char and pyrolysis of mineral components, which led to a further tiny mass loss (as shown in Table 2).[30]

Generally, thermokinetic parameters A and E have a strong correlation with each other, which is called a kinetic compensation effect (KCE), i.e., the change in one parameter inevitably requires a compensatory variation in the other.[31] The KCE is a forceful tool for defining the reaction mechanisms and theoretical implications, which is underestimated and inadequately utilized.[32] Thus, it is worth trying to conduct a KCE analysis of PC combustion for further understanding the difference between raw and preoxidized samples. The KCE can emerge as a linear relationship between $\ln A$ and E, which is described in eq 7

$$\ln A = a + b \cdot E \tag{7}$$

where both constants a and b are the compensation parameters.

Figure 6 describes the plots of $\ln A$ and E evaluated by the Miura−Maki method. The high linear correlation coefficients

https://doi.org/10.1021/acsomega.1c05694
ACS Omega 2022, 7, 1121−1131

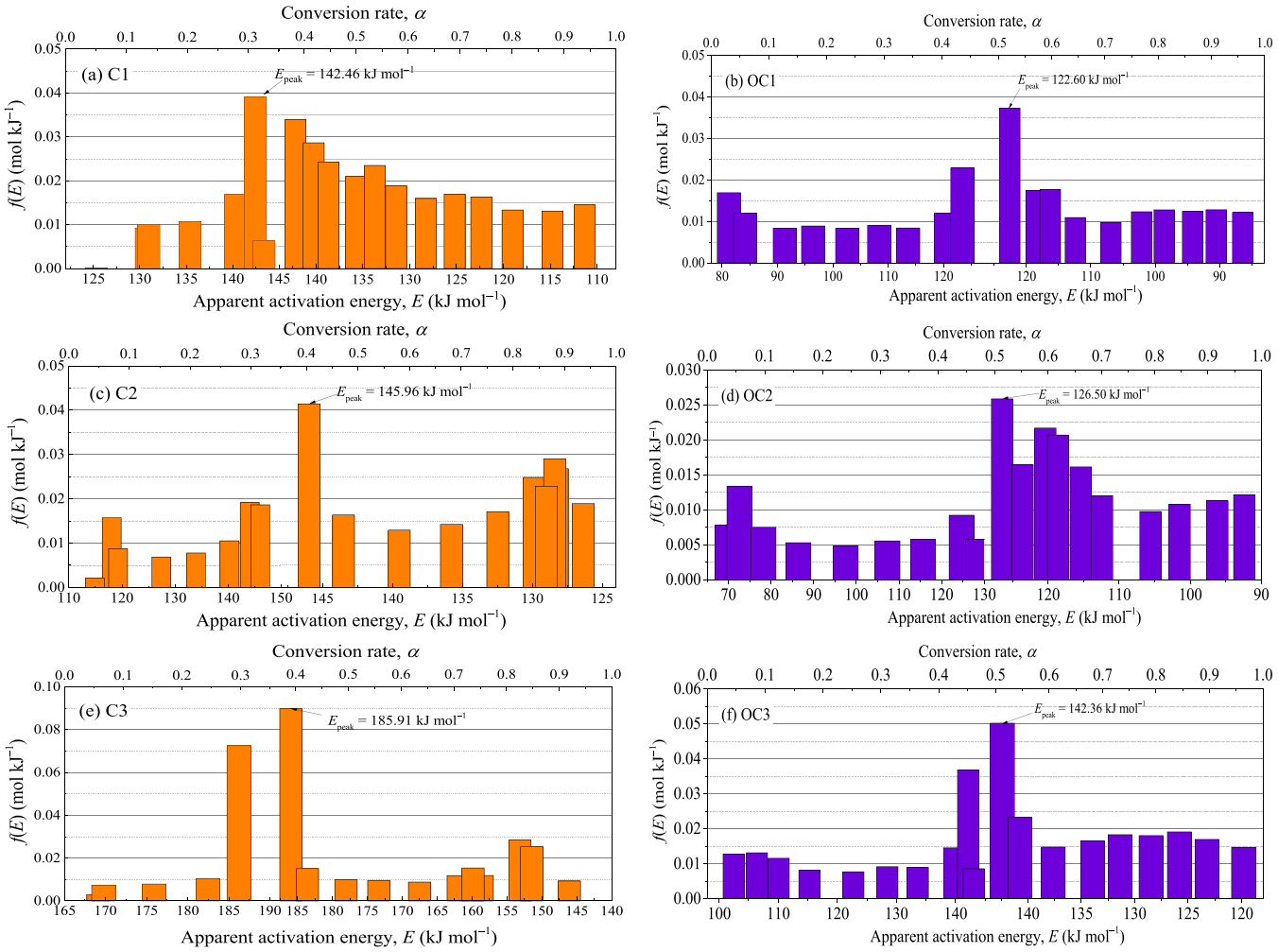

Figure 5. Distribution of apparent activation energies for the pyrolysis and combustion process of raw and preoxidized PC according to a discrete DAEM method: (a) C1, (b) OC1, (c) C2, (d) OC2, (e) C3, and (f) OC3.

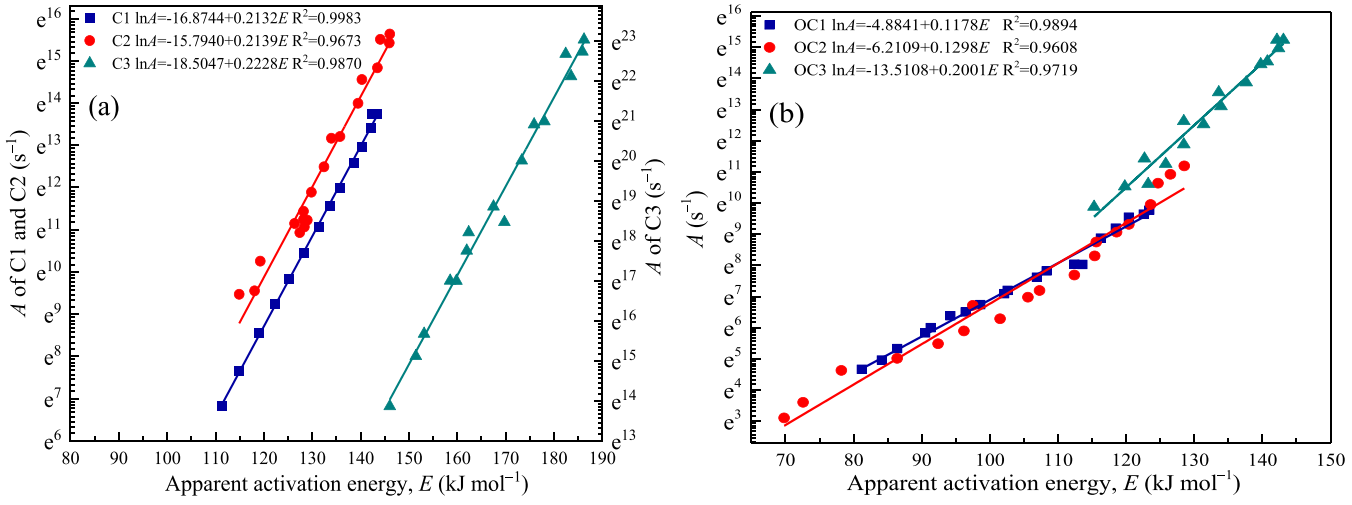

Figure 6. Relationship between ln *A* and *E* determined from the Miura−Maki method for the pyrolysis and combustion process of raw and preoxidized PC: (a) raw samples and (b) preoxidized samples.

(>0.96) strongly suggested the existence of the kinetic compensation effect during pyrolysis and combustion of PC. The compensation parameters *a* and *b* of these samples are also depicted in Figure 6. For the three raw PC, the maximum *b* was observed in sample C3 (0.2228), followed by sample C2 (0.2139), and sample C1 (0.2132) had the minimum value of *b*. Meanwhile, the constants *b* of samples OC1, OC2, and OC3 (0.1178, 0.1298, and 0.2001) were all below those of their corresponding raw samples. Some studies suggested the KCF parameters calculated from *A* and *E* can establish correlation

https://doi.org/10.1021/acsomega.1c05694
ACS Omega 2022, 7, 1121−1131

with the characteristic properties of PC. Yip et al.[33] suggested that the proportionality constant b could be treated as an index of the carbon structural evolution. Thus, it could be deduced that the preoxidation treatment could change the carbon structural form and the types of functional groups (discussed in detail in Section 3.5) and further affect the combustion behavior of PC. In addition, compared to the corresponding raw samples, the intercept constants a of preoxidized samples OC1, OC2, and OC3 decreased by 71, 61, and 27%. The constant a usually denoted the initial surface properties; therefore, the variation of constant a demonstrated that the preoxidation treatment might change the surface properties of PC (e.g., pore size, pore volume, surface area, etc.). To obtain more details of the difference between raw and preoxidized PC, further exploration regarding microcharacteristics of PC was essential.

3.5. Fourier Transform Infrared Spectroscopy (FTIR) Analysis. The band assignments of the main functional groups of FTIR spectra in PC have been determined from researches on coal microstructures.[34] The peak positions in the infrared spectrum and related details of the main functional groups of PC samples are listed in Table 4. FTIR spectrograms of raw and preoxidized samples are presented in Figure 7. Remarkable variations in the spectrograms represented the differences of active functional groups of raw and preoxidized PC. According to the investigations by Ibarra et al.,[36] the infrared spectrum of PC could be divided into four areas: hydroxyl in 3600−3000 cm^{-1}, aliphatic hydrocarbons in 3000−2700 cm^{-1}, oxygen-containing functional groups in 1800−1000 cm^{-1}, and aromatic hydrocarbons in 900−700 cm^{-1}. Generally, defining the boundaries and locations of the absorption peaks is essential for obtaining the relative content of each functional group in PC. Previous studies have suggested that the Gaussian peak fitting method could gain comparatively accurate results, and this method has frequently been utilized for handling the raw data.[37] Thus, the peak fitting analysis was carried out by the PeakFit software in the selected region to semiquantitatively research the variation of main functional groups. The relative content of each functional group in PC was represented semiquantitatively using the integrated area of the peaks gained by the peak fitting process. Figure 8 describes the peak fitting results of the four spectrum parts of sample C1 using the PeakFit software.

Table 4. Band Assignments of the FTIR Spectra of Coal[35]

type	functional groups	location (cm^{-1})	assignment
oxygen-containing functional groups	−OH	3700−3625	free −OH
		3624−3610	−OH bond in hydroxy and ether
		3550−3200	−OH in alcohol/phenol/carboxylic acid or hydrogen bond
	C═O	1880−1785	stretching vibration of C═O
		1780−1630	stretching vibration of C═O
	C−O	1330−900	stretching vibration of C−O
	−COO−	2780−2350	stretching vibration of −COO−
aliphatic hydrocarbons	$-CH_3$	2975−2945	asymmetric stretching vibration of $-CH_3$
		2875 ± 5	symmetrical stretching vibration of $-CH_3$
	$-CH_2$	2930−2880	asymmetric stretching vibration of $-CH_2$
		2855 ± 5	symmetrical stretching vibration of $-CH_2$
		1470 ± 5	variable angle vibration of $-CH_2$
aromatic hydrocarbons	arene	3100−3000	stretching vibration of C−H
		1910−1900	C−C, C−H in benzene
	aromatic ring	1620−1430	stretching vibration of C═C
	substituted benzene	900−675	external deformation vibration of C−H

The relative contents of the main functional groups in all the PC samples are listed in Table 5. It is transparent that the −OH, C═O, and aliphatic hydrocarbon groups of preoxidized PC were below that of the corresponding raw PC, whereas the C−O and −COO− bands increased after oxidation treatment. In addition, the tiny variation of aromatic hydrocarbons was observed between raw and preoxidized PC. The functional groups of the coal structure mainly consist of oxygen-containing functional groups, aromatic and aliphatic hydrocarbons. Oxygen-containing functional groups are the crucial components in coal, which primarily contain the hydroxyl (−OH), carbonyl (C═O), ether (C−O), and carboxyl (−COO−) groups. Aromatic hydrocarbons in coal mainly contain arene (C−H, C−C), aromatic ring (C═C), and substituted benzene (C−H). Aliphatic hydrocarbons in coal mainly contain the methyl ($-CH_3$) and methylene ($-CH_2$).[38]

The −OH bonds mainly include hydroxyl in phenol, alcohol, and water clusters, and the amounts of these groups of preoxidized samples were much less than those of the corresponding raw samples, which was primarily attributed to the loss of moisture in voids and pores of the coal according to the research from Niu et al.[39] The C═O groups and aliphatic hydrocarbons have higher reactivity and could react with oxygen and generate CO_2, CO, and H_2O at a low temperature; thus, the amounts of C═O and aliphatic hydrocarbon groups decreased markedly after oxidation treatment. The C−O bonds primarily exist in phenol, alcohol, ether, and ester. During low-temperature oxidation, active −OH bonds can replace the hydrogen atoms of aromatic or aliphatic hydrocarbon side chains to generate alcohol, or hydroxyl groups are directly connected to the benzene ring to form phenol, which results in the increase of C−O groups. Furthermore, C−O bonds in alkyl ether can be oxidized to −COO− groups. Differences in the strength of both reactions mentioned above caused the increase in C−O groups after oxidation treatment. The change in −COO− groups was also complicated. On the one hand, the side chain of the ether can be oxidized to form a carboxyl group, which is the primary reaction. On the other hand, the −COO− groups can be oxidized into CO and CO_2 emissions. The generation rate of −COO− was higher than its consumption rate, resulting in the fact that the −COO− contents of the preoxidized samples were all larger than those of the corresponding raw samples. The polymerization degree of aromatic hydrocarbons has a remarkable influence on coal maturity, and they consist of arene, aromatic ring, and substituted benzene.[40] The arene and substituted benzene contents decreased slightly through the oxidation treatment, indicating that these two aromatic hydrocarbons participate in the oxidation reaction. Notably, the decrease of substituted benzene amount was primarily caused by the substitution reaction of side chains. The aromatic ring is the core structure of coal, and it is not prone to be oxidized at a low temperature (<120 °C).[41] Thus, the amount of

https://doi.org/10.1021/acsomega.1c05694
ACS Omega 2022, 7, 1121−1131

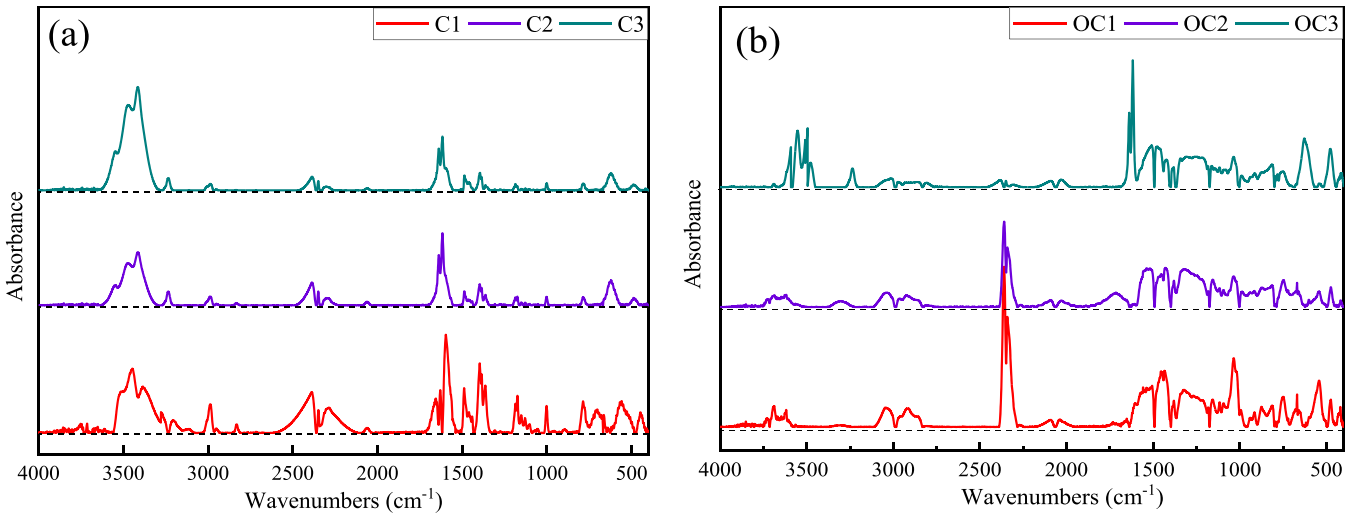

Figure 7. FTIR spectra of raw and preoxidized PC samples: (a) raw samples and (b) preoxidized samples.

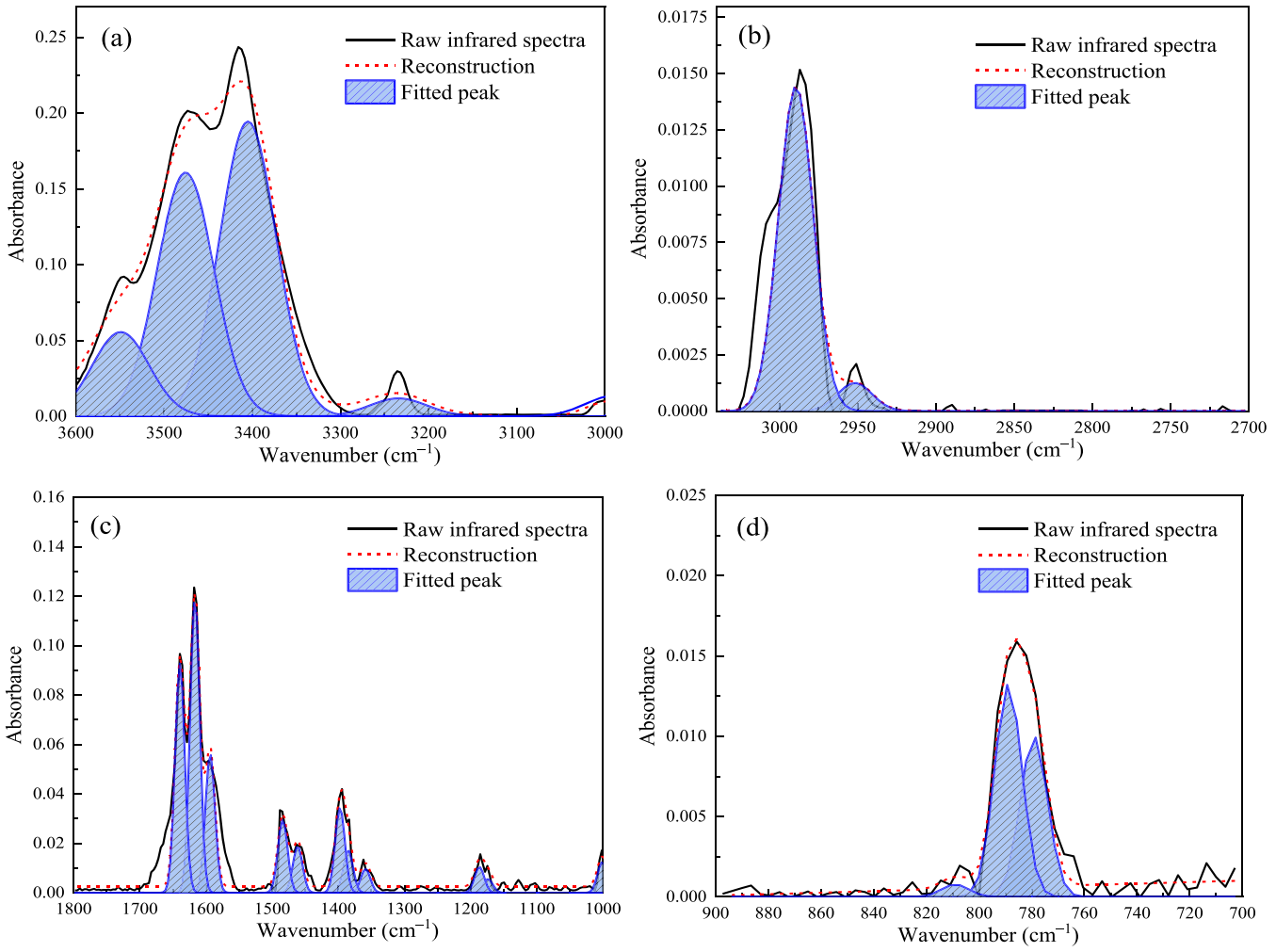

Figure 8. Resolving and construction of FTIR peaks of C1: (a) 3600−3000 cm^{-1}, (b) 3000−2700 cm^{-1}, (c) 1800−1000 cm^{-1}, and (d) 900−700 cm^{-1}.

aromatic ring was constant before and after the preoxidation treatment. In short, the functional group amounts of preoxidized PC were remarkably different from that of raw PC, further resulting in the difference in combustion characteristic and thermokinetic behavior. The preoxidation treatment consumed some functional groups in coal to a certain degree (such as −OH, C═O, and $-CH_3$ groups, etc.), but the increase of C−O and −COO− structures compensated the negative influence from the decrease of abovementioned functional groups on coal combustion. Current research results suggest that the promotive effect of the increase in C−O and −COO− contents on coal

https://doi.org/10.1021/acsomega.1c05694
ACS Omega 2022, 7, 1121−1131

Table 5. Relative Contents of Major Functional Groups in PC Samples

	oxygen-containing functional group				aromatic hydrocarbon			
sample	−OH	C═O	C−O	−COO−	arene	aromatic ring	substituted benzene	aliphatic hydrocarbon
C1	32.16	2.28	1.85	1.59	0.51	7.24	2.63	1.53
OC1	1.16	0.17	7.82	5.53	0.39	7.31	2.35	0.55
C2	13.20	2.93	1.90	2.35	0.92	6.19	3.06	1.69
OC2	1.06	0.78	6.78	3.09	0.74	5.95	2.71	0.61
C3	31.38	3.71	1.96	1.65	0.57	5.81	2.64	1.55
OC3	4.36	0.57	6.86	2.58	0.45	5.72	2.31	0.36

combustion was larger than the inhibition effect of the decrease in −OH, C═O, and aliphatic hydrocarbon contents.

3.6. Summary. The deposited coal dust that has been in a high-temperature circumstance for a long time will gradually be oxidized, and the oxidized coal dust has a relatively lower T_{ig} and T_b compared with the raw coal dust. Furthermore, the combustion performance of these oxidized PC is also better than that of raw PC. At the same α, the E value of oxidized PC is below that of raw PC, which indicates that the oxidized PC has a higher reactivity. In short, the oxidized PC has a higher self-ignition and explosion risk than the raw PC. Therefore, the undesired deposition of coal dust should be avoided during the operation of the milling system in coal-fired boiler, and the positions prone to coal dust deposition should be regularly inspected and timely cleaned up, such as coal mill, coarse powder separator, PC transportation pipeline, etc. In addition, reducing the oxygen concentration in the surrounding is also an excellent method for preventing the ignition and explosion of the deposited PC.[42]

4. CONCLUSIONS

To investigate whether the self-ignition risk of the deposited coal dust is increased under high-temperature airflow, TG and FTIR tests were carried out for contrasting the combustion properties and thermokinetic and microcharacteristics of raw and preoxidized PC samples. Conclusions drawn are as follows:

(1) For each coal sample, the five characteristic temperatures (T_f, T_m, T_{ig}, T_{max}, and T_b) of preoxidized PC were all lower than those of raw PC, which suggested that the preoxidized PC samples were more prone to self-ignition. Both TG and DTG curves moved gradually to the high-temperature zone with the increase of heating rate.

(2) The preoxidized PC had relatively higher values of C_{ig} and S but lower values of C_b than raw PC, which represented that the preoxidized samples could be ignited at a relatively lower temperature but had shorter combustion stage compared with raw PC.

(3) The thermokinetic analysis based on the DAEM method suggested that the E values increased first and then decreased with the increase of α (i.e., coal temperature), and the maximum E value was observed at α = 0.45 (nearby T_{max}). The E values of preoxidized PC were all below those of raw PC at the same α, which indicated that the preoxidized PC required relatively less energy to react and more readily undergoes spontaneous combustion. For each sample, the main abundance distributions of E were more centralized around α = 0.45 (nearby T_{max}).

(4) The preoxidized PC had lower relative amounts of −OH, C═O, and aliphatic hydrocarbon groups and higher C−O and −COO− bonds than raw PC. The partial −OH, C═O, and aliphatic hydrocarbon groups were consumed after the preoxidation treatment, but the increase of C−O and −COO− amounts compensated for the negative influence from the decrease of abovementioned groups on coal combustion.

AUTHOR INFORMATION

Corresponding Author

Yungang Wang − *Key Laboratory of Thermal Fluid Science and Engineering of MOE, School of Energy and Power Engineering, Xi'an Jiaotong University, Xi'an 710049, P. R. China;* orcid.org/0000-0002-2652-9143; Email: ygwang1986@xjtu.edu.cn

Authors

Li Zou − *Key Laboratory of Thermal Fluid Science and Engineering of MOE, School of Energy and Power Engineering, Xi'an Jiaotong University, Xi'an 710049, P. R. China;* orcid.org/0000-0003-2109-0554

Yanyuan Bai − *Key Laboratory of Thermal Fluid Science and Engineering of MOE, School of Energy and Power Engineering, Xi'an Jiaotong University, Xi'an 710049, P. R. China*

Yang Liu − *Key Laboratory of Thermal Fluid Science and Engineering of MOE, School of Energy and Power Engineering, Xi'an Jiaotong University, Xi'an 710049, P. R. China;* orcid.org/0000-0003-0708-6014

Qinxin Zhao − *Key Laboratory of Thermal Fluid Science and Engineering of MOE, School of Energy and Power Engineering, Xi'an Jiaotong University, Xi'an 710049, P. R. China*

Complete contact information is available at: https://pubs.acs.org/10.1021/acsomega.1c05694

Notes

The authors declare no competing financial interest.

ACKNOWLEDGMENTS

This study was supported by the Key Technology Research and Development Program of Shaanxi Province (CN) (Grant Nos. 2018ZDCXL-GY-10-01 and 2018ZDXM-SF-033) and the Innovation Capability Support Project of Shaanxi Province (CN) (Grant No. S2019-ZC-XXXM-0089).

REFERENCES

(1) Song, H.; Liu, G.; Zhang, J.; Wu, J. Pyrolysis characteristics and kinetics of low rank coals by TG-FTIR method. *Fuel Process. Technol.* **2017**, *156*, 454−460.

(2) Qi, G.; Wang, D.; Zheng, K.; Xu, J.; Qi, X.; Zhong, X. Kinetics characteristics of coal low-temperature oxidation in oxygen-depleted air. *J. Loss Prev. Process Ins.* **2015**, *35*, 224−231.

(3) Świątkkowski, B.; Marek, E. Optimisation of pulverized coal combustion in $O_2/CO_2/H_2O$ modified atmosphere−experimental and numerical study. *Energy* **2015**, *92*, 47−53.

https://doi.org/10.1021/acsomega.1c05694
ACS Omega 2022, 7, 1121−1131

(4) Shen, J.; Liu, J.; Xing, Y.; Zhang, H.; Luo, L.; Jiang, X. Application of TG-FTIR analysis to superfine pulverized coal. *J. Anal. Appl. Pyrolysis* **2018**, *133*, 154−161.
(5) Yi, B.; Zhang, L.; Huang, F.; Mao, Z.; Zheng, C. Effect of H_2O on the combustion characteristics of pulverized coal in O_2/CO_2 atmosphere. *Appl. Energy* **2014**, *132*, 349−357.
(6) Ma, L.; Wang, T.; Liu, J.; Fang, Q.; Guo, A.; Zhang, C.; Chen, G. Effect of different conditions on the combustion interactions of blended coals in O_2/CO_2 mixtures. *J. Energy Inst.* **2019**, *92*, 413−427.
(7) Li, Z.; Guo, Z.; Gong, X.; Tang, H. Kinetic characteristics of pulverized coal combustion in the two-phase flow. *Energy* **2013**, *55*, 585−593.
(8) Sung, Y.; Moon, C.; Eom, S.; Choi, G.; Kim, D. Coal-particle size effects on NO reduction and burnout characteristics with air-staged combustion in a pulverized coal-fired furnace. *Fuel* **2016**, *182*, 558−567.
(9) Ren, L.; Deng, J.; Li, Q.; Ma, L.; Zou, L.; Laiwang, B.; Shu, C. Low-temperature exothermic oxidation characteristics and spontaneous combustion risk of pulverised coal. *Fuel* **2019**, *252*, 238−245.
(10) Deng, J.; Zhao, J.; Zhang, Y.; Wang, C. Micro-characteristics of spontaneous combustion of second oxidation with different rank coals. *J. China Coal Soc.* **2016**, *41*, 1164−1172.
(11) Ma, L.; Zou, L.; Ren, L.; Chung, Y.; Zhang, P.; Shu, C. Prediction indices and limiting parameters of coal spontaneous combustion in the Huainan mining area in China. *Fuel* **2020**, *264*, No. 116883.
(12) Wei, G.; Wen, H.; Deng, J.; Li, Z.; Fan, S.; Lei, C.; Liu, M.; Ren, L. Enhanced coalbed permeability and methane recovery via hydraulic slotting combined with liquid CO_2 injection. *Process Saf. Environ. Prot.* **2021**, *147*, 234−244.
(13) Zhang, X.; Li, Q.; Xiao, Y.; Lu, J.; Deng, J. Experiment study on the limit parameters of the forsaken coal spontaneous combustion in the re-oxidation process. *J. Saf. Environ.* **2016**, *16*, 101−106.
(14) Deng, J.; Li, Q.; Xiao, Y.; Shu, C. Experimental study on the thermal properties of coal during pyrolysis, oxidation, and re-oxidation. *Appl. Therm. Eng.* **2017**, *110*, 1137−1152.
(15) Tang, Y.; Wang, H. Experimental investigation on microstructure evolution and spontaneous combustion properties of secondary oxidation of lignite. *Process Saf. Environ. Prot.* **2019**, *124*, 143−150.
(16) Wang, Z.; Hong, C.; Xing, Y.; Li, Y.; Feng, L.; Jia, M. Combustion behaviors and kinetics of sewage sludge blended with pulverized coal: with and without catalysts. *Waste Manage.* **2018**, *74*, 288−296.
(17) Lin, Y.; Ma, X.; Ning, X.; Yu, Z. TGA−FTIR analysis of co-combustion characteristics of paper sludge and oil-palm solid wastes. *Energy Convers. Manage.* **2015**, *89*, 727−734.
(18) Zhang, L.; Duan, F.; Huang, Y. Thermogravimetric investigation on characteristic of biomass combustion under the effect of organic calcium compounds. *Bioresour. Technol.* **2015**, *175*, 174−181.
(19) Cai, J.; Wu, W.; Liu, R. An overview of distributed activation energy model and its application in the pyrolysis of lignocellulosic biomass. *Renewable Sustainable Energy Rev.* **2014**, *36*, 236−246.
(20) Liu, J.; Ma, J.; Luo, L.; Zhang, H.; Jiang, X. Pyrolysis of superfine pulverized coal. Part 5. Thermogravimetric analysis. *Energy Convers. Manage.* **2017**, *154*, 491−502.
(21) He, C.; Tang, C.; Liu, W.; Dai, L.; Qiu, R. Co-pyrolysis of sewage sludge and hydrochar with coals: Pyrolytic behaviors and kinetics analysis using TG-FTIR and a discrete distributed activation energy model. *Energy Convers. Manage.* **2020**, *203*, No. 112226.
(22) Miura, K. A new and simple method to estimate $f(E)$ and $k_0(E)$ in the distributed activation energy model from three sets of experimental data. *Energy Fuels* **1995**, *9*, 302−307.
(23) Deng, J.; Li, B.; Xiao, Y.; Ma, L.; Wang, C.; Laiwang, B.; Shu, C. Combustion properties of coal gangue using thermogravimetry-Fourier transform infrared spectroscopy. *Appl. Therm. Eng.* **2017**, *116*, 244−252.
(24) Li, B.; Chen, G.; Zhang, H.; Sheng, C. Development of non-isothermal TGA-DSC for kinetics analysis of low temperature coal oxidation prior to ignition. *Fuel* **2014**, *118*, 385−391.
(25) Xiao, Y.; Ren, S.; Deng, J.; Shu, C. Comparative analysis of thermokinetic behavior and gaseous products between first and second coal spontaneous combustion. *Fuel* **2018**, *227*, 325−333.
(26) Qi, C.; Zhang, J.; Lin, X.; Liu, Q.; Wang, X. Investigation on pulverized coal combustion behavior by non-isothermic integral thermogravimetry method. *J. Iron Steel Res. Int.* **2011**, *18*, 1−8.
(27) Zhai, X.; Ge, H.; Shu, C.; Obracaj, D.; Wang, K.; Laiwang, B. Effect of the heating rate on the spontaneous combustion characteristics and exothermic phenomena of weakly caking coal at the low-temperature oxidation stage. *Fuel* **2020**, *268*, No. 117327.
(28) López-González, D.; Fernandez-Lopez, M.; Valverde, J.; Sanchez-Silva, L. Kinetic analysis and thermal characterization of the microalgae combustion process by thermal analysis coupled to mass spectrometry. *Appl. Energy* **2014**, *114*, 227−237.
(29) Li, X.; Lv, Y.; Ma, B.; Jian, S.; Tan, H. Thermogravimetric investigation on co-combustion characteristics of tobacco residue and high-ash anthracite coal. *Bioresour. Technol.* **2011**, *102*, 9783−9787.
(30) Xiao, Y.; Lv, H.; Huang, A.; Deng, J.; Shu, C. A new numerical method to predict the growth temperature of spontaneous combustion of 1/3 coking coal. *Appl. Therm. Eng.* **2018**, *131*, 221−229.
(31) Vyazovkin, S.; Burnham, A.; Criado, J.; Perez-Maqueda, L.; Sbirrazzuoli, N.; et al. ICTAC Kinetics Committee recommendations for performing kinetic computations on thermal analysis data. *Thermochim. Acta* **2011**, *520*, 1−19.
(32) Song, H.; Liu, G.; Wu, J. Pyrolysis characteristics and kinetics of low rank coals by distributed activation energy model. *Energy Convers. Manage.* **2016**, *126*, 1037−1046.
(33) Yip, K.; Ng, E.; Li, C.; Hayashi, J.; Wu, H. A mechanistic study on kinetic compensation effect during low-temperature oxidation of coal chars. *Proc. Combust. Inst.* **2011**, *33*, 1755−1762.
(34) Zhao, J.; Wang, W.; Fu, P.; Wang, J.; Gao, F. Evaluation of the spontaneous combustion of soaked coal based on a temperature-programmed test system and in-situ FTIR. *Fuel* **2021**, *294*, No. 120583.
(35) Given, P.; Marzec, A.; Barton, W.; Lynch, L.; et al. The concept of a mobile or molecular phase within the macromolecular network of coals: A debate. *Fuel* **1986**, *65*, 155−163.
(36) Ibarra, J.; Munoz, E.; Moliner, R. FTIR study of the evolution of coal structure during the coalification process. *Org. Geochem.* **1996**, *24*, 725−735.
(37) Ge, L.; Zhang, Y.; Xu, C.; Wang, Z.; Zhou, J.; Cen, K. Influence of the hydrothermal dewatering on the combustion characteristics of Chinese low-rank coals. *Appl. Therm. Eng.* **2015**, *90*, 174−181.
(38) Niu, Z.; Liu, G.; Yin, H.; Wu, D.; Yousaf, B.; Wang, C.; et al. In-situ FTIR study of reaction mechanism and chemical kinetics of a Xundian lignite during non-isothermal low temperature pyrolysis. *Energy Convers. Manage.* **2016**, *124*, 180−188.
(39) Niu, Z.; Liu, G.; Yin, H.; Wu, D.; Zhou, C. Investigation of mechanism and kinetics of non-isothermal low temperature pyrolysis of perhydrous bituminous coal by in-situ FTIR. *Fuel* **2016**, *172*, 1−10.
(40) Ma, L.; Yu, W.; Ren, L.; Qin, X.; Wang, Q. Micro-characteristics of low-temperature coal oxidation in CO_2/O_2 and N_2/O_2 atmospheres. *Fuel* **2019**, *246*, 259−267.
(41) Ma, L.; Zou, L.; Ren, L.; Wang, J.; Wang, W. Reactivity and spontaneous combustion characteristics of high-sulphur coal during low-temperature oxidation. *Int. J. Oil Gas Coal Technol.* **2019**, *21*, 375−389.
(42) Deng, J.; Ren, L.; Ma, L.; Lei, C.; Wei, G.; Wang, W. Effect of oxygen concentration on low-temperature exothermic oxidation of pulverized coal. *Thermochim. Acta* **2018**, *667*, 102−110.

https://doi.org/10.1021/acsomega.1c05694
ACS Omega 2022, 7, 1121−1131